ISSN No: 2348-4845
International Journal & Magazine of Engineering, Technology, Management and Research
A Peer Reviewed Open Access International Journal

Increasing Electrical Damping in Energy Harnessing Transducers

B Renuka
B.Tech Scholar,
Department of Electrical and Electronics Engineering,
Siddhardha Institute of Engineering and Technology,
Vinobha Nagar, Ibrahimpatnam, Hyderabad,
Telangana-501506, India.

B Dhanadeepika
Assistant Professor,
Department of Electrical and Electronics Engineering,
Siddhardha Institute of Engineering and Technology,
Vinobha Nagar, Ibrahimpatnam, Hyderabad,
Telangana-501506, India.

Abstract

Energy and power in tiny batteries are often insufficient to sustain the demands of a wireless microsystem for extended periods. The transducers are viable alternatives because they draw power from a vast tank-free supply of ambient kinetic energy in vibrations. Unfortunately, small devices alone seldom dampen vibrations enough to fully harness what is available, which is why investing energy to increase the electrical damping force that transducers impose is so important. This paper introduces and evaluates three investment schemes and 0.35-μm CMOS switched-inductor circuits that increase this force to generate more output power.

I. Introduction

Energy from ambient sources (as in Fig. 1) can extend the operational life of a microsystem by recharging a depleting battery. State-of-the-art microscale transducers, however, only generate μW's, of which power conditioning circuits consume a portion [2]. Fortunately, electrical energy E_E increases with electrical damping force, which as this paper demonstrates, can increase with initially invested energy E_{INV}. To consider this in more detail, Sections II, III, IV and V discuss how investing energy increases output power in electromagnetic, electrostatic, and piezoelectric transducers, drawing relevant conclusions in Section VI.

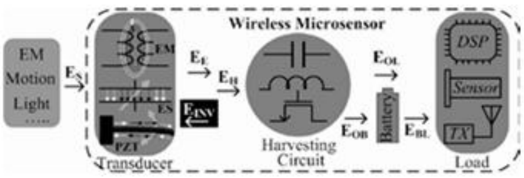

Fig. 1. Sample harvesting wireless microsystem.

II. Electrical Damping

A. Theoretical Behavior

One such alternative for increased damping is to introduce damping on the electrical side rather than the mechanical side of the system's drive motor. Using a one degree-of-freedom device modeling a virtual wall as an example, it is seen that this can be accomplished by inserting an electrical resistance in parallel with the motor (Fig. 1b) [3-5]. After analyzing the constitutive relations of such a system it is seen that the equivalent mechanical damping that this electrical system adds is

$$B_{eq} = \frac{K_t^2}{(R_1 + R_m)}. \quad (1)$$

where Kt is the motor's torque constant, Rm is the motor's internal resistance, and R1 is the added parallel resistance.

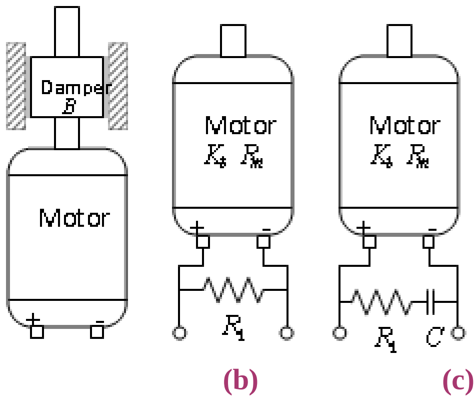

Figure 2: A mechanically damped system (a) and two electrically damped systems; one without (b) and one with frequency dependence (c).

With only an added resistor the electrical system acts just as a mechanical damper, dissipating energy throughout the device's range of motion.

ISSN No: 2348-4845
International Journal & Magazine of Engineering, Technology, Management and Research
A Peer Reviewed Open Access International Journal

An improvement can be made, however, by adding a capacitor in series with the added parallel resistance (Fig. 1c). This makes the electrical damping frequency dependent. The values of resistance and capacitance can be chosen to give the system a cutoff frequency around the normal bandwidth of human hand motion (a relatively small 2 Hz [6-8] to 4.5 Hz [9]). Thus, away from any constraints, when movement is governed almost entirely by inputs from the human user, the system acts as if there is no extra damping. When a high frequency event occurs, as in impacting a virtual wall, the electrical damping can serve to prevent the energy growth that leads to limit cycle oscillations and other instabilities. This method of providing real physical damping, therefore, eliminates the need for unwieldy mechanical dampers while also simplifying the control structure and device design by doing away with the need for negative virtual damTop ifnugr.t her understand the behavior of an electrically damped system, a one degree-of-freedom device with electrical damping can be modeled (as in Fig. 2) and the following system transfer function can be analyzed. This model omits friction and structural compliance for simplicity.

$$\tau(s) = K_t n\left[\frac{R_1 Cs+1}{LCs^2+(R_1+R_m)Cs+1}\right]I(s) - \left[\frac{K_t^2 n^2 Cs}{LCs^2+(R_1+R_m)Cs+1}+n^2(B+Js)\right]v(s) \quad (2a)$$

$$\tau(s) = A(s)I(s) - Z(s)v(s) \quad (2b)$$

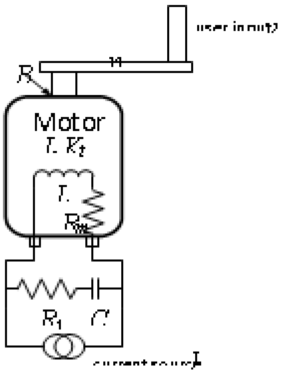

Figure 3: Model used for analyzing the theoretical behavior of a one degree-of-freedom haptic display with electrical damping

Here, it is seen that the torque, τ, is responsive to two inputs: the current from the amplifier, I, and the angular velocity of the motor shaft, v. The system characteristics of the device used in testing (described in Section 3) can be substituted into (2a) and the resulting frequency responses can be plotted to obtain a more complete picture of haptic display performance. First, velocity is assumed to be zero and the resulting plot of the magnitude of A(s), Fig. 3a, shows the frequency response of torque to a current input (specific parameter values are given in Section 3). It is desirable to have this plot constant, or as close as possible, because any shift in this effective "torque constant" corresponds [10] to a change in the ability of a commanded current to output a desired torque. While the goal of electrical damping is to dissipate unwanted energy at high frequencies, the ability to control the haptic display with current commands of reasonable magnitude, at all frequencies, must be maintained. Magnitude of Frequency Response for A(s), the Torque/Current Transfer Function for Electrical Damping = 0.00755 Nms/rad

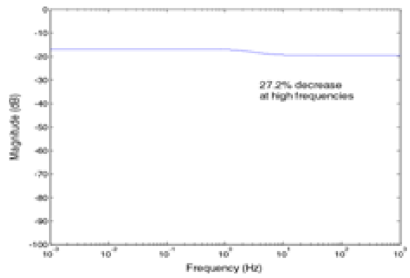

(a)

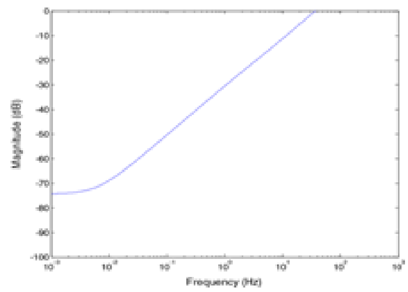

(b)

Figure 4: Magnitude portions of the Bode plots for the transfer functions A(s) (a) and Z(s) (b) for a system with 0.00755 Nm/(s/rad) of electrical damping

ISSN No: 2348-4845
International Journal & Magazine of Engineering, Technology, Management and Research
A Peer Reviewed Open Access International Journal

If current rather than velocity is assumed zero, the magnitude of Z(s), the transfer function from velocity input to torque output can be plotted (Fig. 3b). This magnitude can be further broken down into its real and imaginary components (see Fig. 4). Re{Z(s)} corresponds to the effective damping of the system while Im{Z(s)}/ω represents the apparent inertia felt at the device output [[11-13]. From these plots it is clear that significant additional damping is added to the system at high frequencies, and only high frequencies. Also, motions at low frequencies experience only a slight increase in system inertia due to the added parallel capacitance. Thus, electrical damping can aid in stabilizing high frequency events like an impact with a virtual wall, while not hindering a user's unconstrained motion away from the boundary. Effective Damping vs. Frequencfor Electrical Damping = 0.00755 Nms/rad

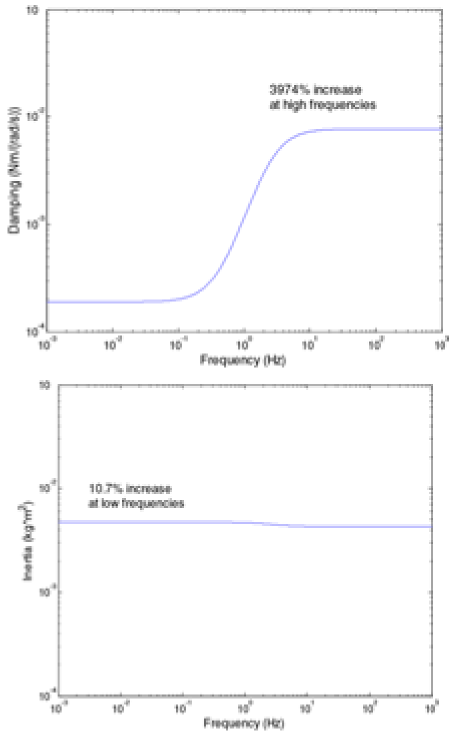

(a) Apparent Inertia vs. Frequency (b)
Figure 5: Theoretical effective damping (a) and apparent inertia (b) obtained from Z(s) for a system with 0.00755 Nm/(s/rad) of electrical damping

II. ELECTROSTATIC TRANSDUCERS

A variable capacitor C_{VAR} having one physically suspended plate that moves under the influence of environmental motion can harvest energy. In voltage-constrained (VC) harvesting, because capacitance-voltage product represents charge, maintaining the voltage across C_{VAR} constant when vibrations separate its plates (i.e., decrease capacitance) reduces its charge, which means C_{VAR} produces energy. In charge constrained (QC) operation, since linear variations in C_{VAR}'s voltage causes squared changes in energy (i.e., E_C is $0.5C_{VAR}v_C^2$), fixing C_{VAR}'s charge by keeping it open when vibrations decrease C_{VAR} raises v_C, so v_C^2 increases surpass linear reductions in C_{VAR} to produce a net energy gain.

A. Increasing Electrical Damping

In both VC and QC operation, the system invests energy at the beginning of each cycle to pre-charge C_{VAR}. Some or all of this charge remains on C_{VAR}'s plates through the harvesting phase to establish an electrostatic attraction that opposes (and damps) the physical movement of the suspended plate. Vibrations, as a result, produce more energy when this electrical damping force (F_{DE}) is higher [14-15]. In the presence of overpowering mechanical damping forces (when Z_S overwhelms $k_C^2Z_E$ in Fig. 2), F_{DE} has little impact on the displacement x(t) of C_{VAR}'s plates [4], which means raising F_{DE} draws more electrical energy from vibrations. Therefore, because F_{DE} increases with the square of C_{VAR}'s voltage v_C, as does C_{VAR}'s E_C, higher voltages through the harvesting phase induce more electrical damping in the transducer and, as a result, produce more output energy E_H:

$$E_H = \int F_{DE}dx \propto \int \frac{v_C^2}{x(t)^2}dt \propto \int \frac{E_C}{x(t)^2}dt.$$

This means that keeping v_C as close to C_{VAR}'s breakdown voltage (V_{MAX}) throughout the harvesting period generates more energy than otherwise, which is why VC harvesting at or near V_{MAX} spawns more energy than in QC operation, where v_C rises and nears V_{MAX} only at the end of the cycle [9].

ISSN No: 2348-4845
International Journal & Magazine of Engineering, Technology, Management and Research
A Peer Reviewed Open Access International Journal

B. Voltage-clamping Capacitor

Constraining C_{VAR}'s voltage with a 2.7 – 4.2-V li-ion battery [10] through the harvesting cycle is one way of extracting energy from motion directly into a battery (V_{BAT}). The advantages of this are that no additional capacitors or energy transfers, which are lossy, are necessary. Unfortunately, V_{BAT} is not the maximum voltage C_{VAR} can sustain, which means C_{VAR} does not draw as much energy as its breakdown voltage allows. So, at the cost of silicon or printed-circuit-board (PCB) area, a large clamping capacitor C_{CLAMP} (of up to 1 nF) that constrains C_{VAR} (e.g., 50 – 250 pF) above V_{BAT} near V_{MAX}, as in Fig. 6, can harness sufficient energy to overcome losses in an additional energy-transfer phase.

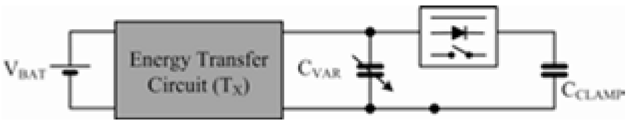

Fig. 6. Constraining C_{VAR}'s voltage with a clamping capacitor.

Permanent Connection:

In hard-wiring C_{CLAMP} to C_{VAR} [9], energy-transfer circuit (i.e., T_X) first invests energy E_{INV} from battery V_{BAT} to pre-charge both C_{VAR} and C_{CLAMP} close to V_{MAX}. Then, once the harvesting cycle ends, T_X must fully discharge both capacitors, before C_{VAR} uses remnant energy to help pull its plates together. Because C_{CLAMP} is much higher than C_{VAR} (to ensure C_{CLAMP} clamps C_{VAR} near V_{MAX} when C_{VAR} changes), T_X transfers considerably more energy (E_{INV} and E_H) than it harvests (E_H), so conduction losses are correspondingly higher.

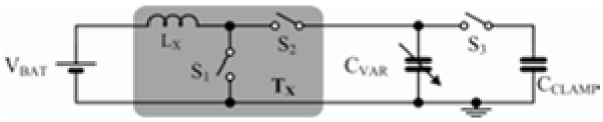

Fig. 7. Proposed electrostatic harvester.

Asynchronous Connection:

T_X in [11] pre-charges C_{VAR} to a fraction of V_{MAX} so mechanical energy can raise C_{VAR}'s voltage to a diode voltage above C_{CLAMP}'s initially high voltage (near V_{MAX}) before driving charge into C_{CLAMP}.

The interface circuit then transfers harnessed energy in C_{CLAMP} to V_{BAT}. Although T_X transfers less energy because C_{CLAMP} keeps its initial charge, the diode dissipates power and C_{VAR}'s voltage is considerably below V_{MAX} for a substantial portion of the harvesting period.

Managed Connection [Proposed]:

Alternatively, T_X in Fig. 7 charges C_{VAR} to C_{CLAMP}'s initial voltage (near V_{MAX}), and once done, the controller closes switch S_3 to steer mechanical energy extracted into C_{CLAMP}. T_X then discharges C_{VAR} into V_{BAT} before vibrations push its plates together, and deenergizes C_{CLAMP} with C_{VAR} (via S_3) less often, when C_{CLAMP} reaches V_{MAX}. As such, C_{VAR} remains close to V_{MAX} through the entire harvesting phase and S_3 dissipates less power than the diode in [11] (because its terminal voltages are considerably lower). Adding intelligence to manage the precharge process and the ensuing connection this way, however, requires energy, which represents a loss to the system.

C. Performance and Limitations

The major drawback to C_{CLAMP} is its impact on integration. Unfortunately, reducing capacitance increases C_{CLAMP}'s voltage variation (through the harvesting phase), so its voltage must start further below V_{MAX} (at V_{INI} in Fig. 8) to keep C_{CLAMP} from breaking down. As a result, C_{VAR} harvests less energy per cycle, as E_{OUT} in Fig. 8 shows below 100 pF for a 0.35-µm CMOS circuit with 40-V devices. Interestingly, increasing C_{CLAMP} when permanently connected to C_{VAR} (e.g., above 100 pF in Fig. 8) does not always increase E_{OUT}. This happens because T_X transfers more charge to raise C_{CLAMP} near V_{MAX}, which means additional conduction losses negate the gains of increased electrical damping forces. The circuit proposed in Fig. 7, however, transfers substantially less energy because C_{CLAMP} retains its initial charge through all phases.

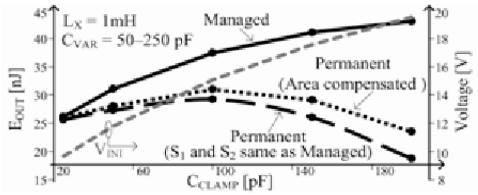

Fig. 8. Simulated output energy across clamping capacitances.

One difference between the two connection strategies is the presence of S_3, which requires silicon area. Removing S_3 and dedicating its area to other switches decreases the resistance across (and conduction losses in) the system, raising E_{OUT}. Reducing resistances by this amount, however, does not compensate for the losses that transferring all of C_{CLAMP}'s charge incurs, as E_{OUT} in Fig. 8 shows. Still, controlling S_3 requires quiescent and switching energy not accounted for in Fig. 8. As a result, managing the connection is better only if conduction losses with a permanent connection exceed controller losses, which is more likely when C_{CLAMP} is higher because higher capacitance requires more energy to charge.

IV. PIEZOELECTRIC TRANSDUCERS

A. Battery-coupled Damping

Piezoelectric transducers (PZT) generate charge in response to mechanical vibrations. When open-circuited, the resulting current energizes and de-energizes the capacitance across the surfaces of the device (C_P) and supplies the parasitic leakage across the same (via R_P). Cascading a full-wave rectifier and a battery V_{BAT} (as in Fig. 9, but without S_{RE} and L_{RE}) steers charge away from C_P into V_{BAT} when PZT current i_P charges C_P above the barrier voltage that conducting diodes and V_{BAT} establish (i.e., $2V_D + V_{BAT}$). V_{BAT} can harness more energy when MOSFETs replace the diodes because the barrier is lower, but only after i_P charges C_P above V_{BAT}.

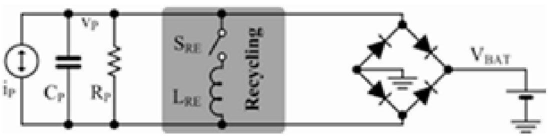

Fig. 9. Recycling inductor L_{RE} into a full-wave rectifier.

When unloaded, to be more specific, i_P charges C_P from negative to positive open-circuit voltages $-V_{OC}$ to V_{OC} (by $2V_{OC}$) with charge Q_{OC}, which is $2V_{OC}C_P$. When loaded, the rectifier conducts to V_{BAT} the portion of Q_{OC} that would have charged open-circuited C_P above $|V_{BAT}|$ to $|V_{OC}|$, so V_{BAT} harnesses the difference twice (every half cycle) as

$$E_H = 2(Q_{OC} - 2V_{BAT}C_P)V_{BAT} = 4C_P(V_{OC} - V_{BAT})V_{BAT}, \quad (6)$$

The peak of which happens at $C_P V_{OC}^2$ when V_{BAT} is $0.5V_{OC}$ [14]. Here, vibrations supply and absorb the energy with which they charge and discharge C_P between V_{BAT} and $-V_{BAT}$.

Recycling Inductor:

L_{RE} in Fig. 9 [15]–[16] increases E_H by recycling C_P's energy at V_{BAT} to energize C_P in the other direction to $-V_{BAT}$. That is, after the positive half cycle, S_{RE} closes and L_{RE} de-energizes C_P and subsequently (through resonance) supplies the energy L_{RE} stored in the process to charge C_P to $-V_{BAT}$. In this manner, C_P draws no mechanical energy to charge to V_{BAT} and $-V_{BAT}$, so collects all of Q_{OC} as:

$$E_H' = 2Q_{OC}V_{BAT} = 2(2V_{OC}C_P)V_{BAT} = 4C_P V_{OC} V_{BAT}.$$

S_{RE} and the circuit used to control S_{RE} dissipate power, so the energy C_P requires to charge between $-V_{BAT}$ and V_{BAT} every half cycle, which is $2(0.5C_P(2V_{BAT})^2)$ or $4C_P V_{BAT}^2$, should surpass these losses. In the end, drawing energy from vibrations amounts to damping them. With a rectifier, since the transducer ejects Q_{OC} near V_{BAT}, and output energy per half cycle is $Q_{OC}V_{BAT}$, V_{BAT} ultimately limits the electrical damping force from which the transducer harvests energy.

Reinvesting Energy [Proposed]:

Increasing output energy is possible by reinvesting the energy gained in half the cycle (rather than depositing into V_{BAT}) to increase the electrical damping force in the other half. For example, redirecting all the energy C_P draws from vibrations to charge by $2V_{OC}$ to charge C_P in the opposite direction pre-charges C_P to $-2V_{OC}$ so vibrations in the negative half cycle further charge C_P by another $2V_{OC}$ to $-4V_{OC}$.

Because the energy in a capacitor increases with the square of its voltage, harnessing what C_P stores at $-4V_{OC}$ once per cycle produces more than drawing C_P's energy twice at half that voltage, at $2V_{OC}$ and $-2V_{OC}$:

$$E_H''' = 0 + 0.5C_P(-4V_{OC})^2 = 8C_PV_{OC}^2.$$

To realize this, after CP_{PK} in Fig. 11 senses that v_P peaks, M_{N1}–M_{N2} and M_{N3}–M_{N4}, which implement S_I and S_N in Fig. 10, close for L_HC_P's half resonance period so that C_P discharges into L_H and L_H subsequently de-energizes back into C_P. Once CP_{PK} senses that open-circuited C_P peaks in the opposite direction, S_I and S_N close to discharge C_P into L_H and S_I alone opens to de-energize L_H into V_{BAT} through M_{PDI}, which together with CP_{DI}, emulates diode D_I.

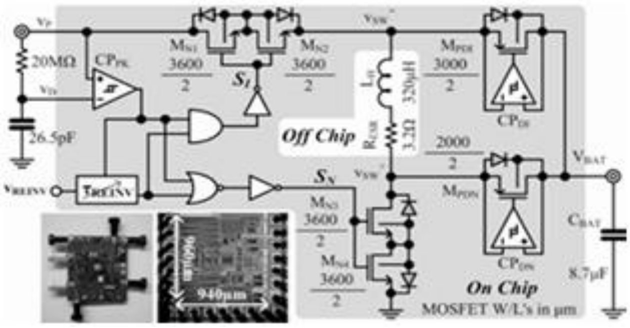

Fig. 11. Prototyped 2-µm BiCMOS re-investing, rectifier-free harvester.

C. Experimental Validation

The prototyped 2-µm BiCMOS harvester tunes the time that S_I and S_N connect (τ_{REINV}) externally with v_{REINV}. , τ_{REINV} extends beyond L_HC_P's quarter resonance period to a half to reinvest L_H's energy back in C_P. When τ_{REINV} is less than L_HC_P's half resonance period, S_N opens early and L_H drains remnant energy into V_{BAT} via M_{PDN}, which with CP_{DN}, implements D_N. Once tuned, shaking a 44 × 13 × 0.4-mm^3 piezoelectric transducer charged C_P and L_H then recycled C_P's energy at 1.02 V to pre-charge C_P in the opposite direction to –0.36 V, as Fig. 12a shows. Vibrations then charged C_P further to –1.9 V before L_H de-energized C_P into C_{BAT}. After 2.5 s of repeated cycles, C_{BAT} charged from 2.68 to 4.36 V, as Fig. 12b corroborates.

Without reinvesting energy, C_P charged to 1.4 V and –1.2 V to energize C_{BAT} from 2.68 to 4.36 V in 3 s, which under similar conditions, means reinvesting energy produced 20% more output power.

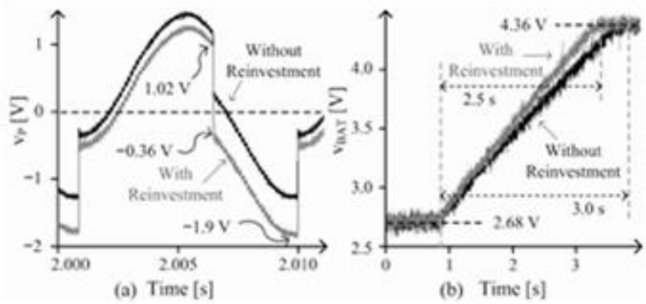

Fig.12. Measured C_P and C_{BAT} charge profiles with and without reinvestment.

D. Performance and Limitations

Notice CP_{PK} is late in detecting v_P's peaks, so before L_H can de-energize C_P, vibrations absorb some of C_P's energy (in both cases shown). Also note that L_H's reinvestment in C_P is unable to charge C_P to –1.02 V because conducting switches (S_N and S_I) and L_H's equivalent series resistance R_{ESR} dissipate some of that energy. This is critical because reducing C_P's negative peak voltage has a squared impact on C_P's peak energy, which is what the system harvests.

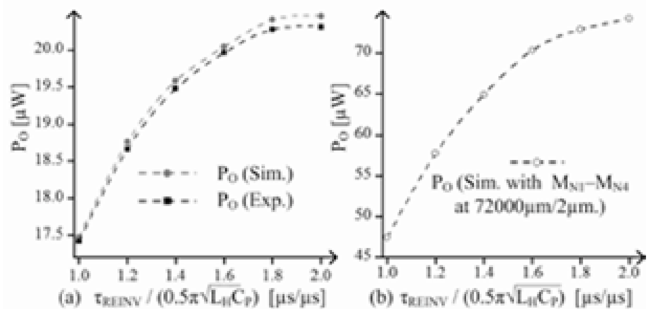

Fig. 13. Experimental and simulated output power across investment time.

Interestingly, as the experimental results of Fig. 13a show, increasing the investment in C_P produces diminishing returns in P_O. This results because transferring more energy through the switches and L_H's R_{ESR} also increases conduction losses to the point they overwhelm reinvestment gains.

ISSN No: 2348-4845
International Journal & Magazine of Engineering, Technology, Management and Research
A Peer Reviewed Open Access International Journal

Enlarging the FETs to lower their resistances balances losses and therefore raises P_O, as the simulated traces of Fig. 13b show. With twenty times (20×) larger FETs for S_N and S_I (at 72000µm/2µm), in fact, fully investing C_P's positive energy into the negative phase raised simulated P_O by 56% from 47.4 µW to 74.2 µW. Ultimately, however, FET losses vary with input power, process, and temperature, but not mismatch.

V. CONCLUSIONS

The experimental results of the piezoelectric transducer and the simulated results of the electromagnetic and electrostatic cases show that investing energy into the system increases output power P_O. This is important because the coupling factors of tiny transducers and transponding inductors are substantially low, which means P_O is also low. The idea here is to invest energy to raise the electrical damping force against which motion, magnetic fields, etc. work. This way, transducers draw more energy from the environment. The circuit components that transfer the investment, however, consume power, limiting the extent to which increased investments raise P_O. Still, increasing P_O this way, beyond reducing losses in the system, expands the functional reach of miniaturized systems to more practical levels.

REFERENCES

[1] G. Chen et al., "Circuit Design Advances for Wireless Sensing Applications," Proc. IEEE, vol. 98, no. 11, pp. 1808-1827, Nov. 2010.

[2] R.J.M. Vullers et al., "Micropower energy harvesting," Solid-State Electronics, vol. 53, no. 7, pp. 684 – 693, Jul. 2009.

[3] S. D. Senturia, "Energy-conserving transducers" in Microsystem Design, New York: Springer, 2001, pp. 125-145.

[4] P.D. Mitcheson et al., "Architectures for vibration-driven micropower generators," J. Microelectromech. Syst., vol.13, no. 3, pp. 429- 440, Jun. 2004.

[5] L. Xun and S. Y. Hui, "Simulation study and experimental verification of a universal contactless battery charging platform with localized charging features," IEEE Trans. Power Electron, vol. 22, pp. 2202-2210, Nov. 2007.

[6] M. Kiani and M. Ghovanloo, "An RFID-based closed-loop wireless power transmission system for biomedical applications," IEEE Trans. Circuits Syst. II, vol. 57, pp. 260-264, Apr. 2010.

[7] M. W. Baker and R. Sarpeshkar, "Feedback analysis and design of RF power links for low-power bionic systems," IEEE Trans. Biomed. Circuits Syst., vol. 1, pp. 28-38, 2007.

[8] C. Chih-Jung et al., "A study of loosely coupled coils for wireless power transfer," IEEE Trans. Circuits Syst. II, vol. 57, pp. 536-540, Jul. 2010.

[9] S. Meninger et al., "Vibration-to-electric energy conversion," IEEE Trans. Very Large Scale Integr. (VLSI) Syst., vol. 9, pp. 64-76, Feb. 2001.

[10] E. O. Torres and G. A. Rincon-Mora, "A 0.7-µm BiCMOS electrostatic energy-harvesting system IC," IEEE J. Solid-State Circuits, vol. 45, pp. 483-496, Feb. 2010.

[11] B. C. Yen and J. H. Lang, "A variable-capacitance vibration-to-electric energy harvester, " IEEE Trans. Circuits Syst. I, vol. 53, pp. 288-295, Feb. 2006.

[12] D. Kwon et al., "Harvesting ambient kinetic energy with switchedinductor converters," IEEE Trans. Circuits Syst. I, vol. 58, no. 7, pp.1551–1560, July 2011.

[13] H. Lam et al., "Integrated low-loss CMOS active rectifier for wirelessly powered devices," IEEE Trans. Circuits Syst. II, vol. 53, no. 12, pp. 1378–1382, Dec. 2006.

[14] G.K. Ottman et al., "Adaptive piezoelectric energy harvesting circuit for wireless remote power supply," IEEE Trans. Power Electron., vol. 17, no. 5, pp. 669–676, Sep. 2002.

[15] E. Lefeuvre et al., "A comparison between several vibration-powered piezoelectric generators for standalone systems," Sensors and Actuators A, vol. 126, pp. 405–416, 2006.